ANALYSIS OF A BI-LAYERED CAPILLARY EVAPORATOR WICK

Paulo Henrique Dias dos Santos, paulosantos@labcet.ufsc.br
Amir Antônio Martins Oliveira, amir.oliveira@gmail.com
Edson Bazzo, ebazzo@emc.ufsc.br

Federal University of Santa Catarina, Departament of Mechanical Engineering, LabCET - Laboratory of Combustion and Thermal Systems Engineering - Campus Universitário, 88.040-900, Florianópolis, SC, Brazil

Abstract. *Capillary evaporators are devices used in the thermal control of satellites and electronic systems in general. The main component of these devices is the wick that promotes the circulation of the working fluid by capillary effect. Here, a numerical evaluation of the heat and mass transfer of a capillary evaporator with a flat bi-layered porous wick is presented. The wick, in the shape of a flat disc, is assembled between the liquid feeding channel and the vapor chamber. The upper part of the wick, where the working fluid evaporates, is heated by an external heat flux. The mass and heat transfer problems are modeled by the equations of energy and mass conservation. The fluid is assumed incompressible, local thermal equilibrium prevails, Darcy's Law is used to model the viscous flow within the porous medium and the equations are numerically solved using the finite volume method. The model allows to verify the effect of design variables in the performance of the capillary evaporator and it can be used as an useful tool for the design of capillary pumping systems.*

Keywords*: Capillary Evaporator, Heat Pipes, CPL, LHP.*

1. INTRODUCTION

Capillary pumping systems are devices used in the thermal control of satellites and electronic components in general. In the last decades, they have been gaining acceptance in the aerospace community because of their performance advantages, unique characteristics of operation and the success in operation in recent flight experiments. The main component of these devices is the capillary evaporator which contains the porous structure that promotes the working fluid circulation by capillarity. Therefore, the pumping of the working fluid does not consume electric power. Another advantage of these devices is the absence of movable parts.

Many studies have been focused on the analysis of the heat transfer within the capillary evaporators. Demidov and Yatsenko (1994) formulated the heat transfer problem in the porous structures of capillary pumping loop (CPL). They developed a numerical procedure and studied the growth of the vapor zone as the system thermal load is varied. Figus et al. (1999) also presented a numerical solution for the problem proposed by Demidov and Yatsenko (1994). They modeled the problem using continuous (Darcy) and pore network models. The results of the pore network model are approximately identical to those of continuous model for an extremely narrow pore size distribution. A similar problem was also studied by Cao and Faghri (1994a). They obtained analytic solutions for the velocity and temperature fields. However, differently of Demidov and Yatsenko (1994) and Figus et al. (1999), they considered a wick completely saturated by liquid, with the evaporation front stabilizing in the external surface of the wick. They concluded that the results obtained are of relevance for the project of capillary evaporators. Cao and Faghri (1994b) also published an extension of their previous paper, which presents an analysis of a three-dimensional geometry, where the two-dimensional flow of the liquid through the porous media and three-dimensional flow of the vapor through the grooves were considered. They concluded that reasonably accurate results can be obtained by a simplified two-dimensional model, especially when the vapor velocities are small for some types of working fluids, such as Freon-11 and ammonia.

Santos et. al. (2008) obtained an analytical solution for the heat and mass transfer problem as proposed by Cao and Faghri (1994a). They analyzed different types of wicks, working fluids and the variation of some geometric parameters. They concluded that the decrease of the wick thickness increased the capillary limit, however increased both the temperature in the area underneath the fin and the heat flux to the feeding liquid channel. As expected, they also noticed that the smaller the thermal conductivity, the greater the temperatures in the area underneath the fin. They also concluded that the boundary conditions in the vapor outlet surface should be improved to match better with reality.

This paper presents an extension of Santos et. al. (2008). Here, a numerical evaluation of heat and mass transfer of a capillary evaporator with a flat porous wick is presented. The model was used to simulate the heat and mass transfer within a wick with two layers with different thermophysical properties. The mass and heat transfer problems are modeled by the equations of energy and mass conservation. The fluid is assumed incompressible, local thermal equilibrium prevails and Darcy's Law is used to model the viscous flow within the porous medium and the equations are numerically solved using the finite volume method. The model allows to verify the effect of design variables in the performance of the capillary evaporator and can be used as an useful tool for the design of capillary pumping systems. Furthermore, the model allows the test of the onset of drying underneath the fin, defining the limit for the application of the model that considers the wick to be fully saturated with liquid.

2. PROBLEM FORMULATION

The geometry of interest in this paper is shown in Fig. 1a. This figure depicts a bi-layered porous wick. This capillary evaporator was developed in the Laboratory of Combustion and Thermal Systems Engineering (LABCET/UFSC) to be tested in microgravity, at the International Space Station (ISS). The capillary evaporator is part of a CPL which is composed, besides the capillary evaporator, by a condenser, a sub-cooler, a reservoir and liquid and vapor transport lines, according to Fig. 1b.

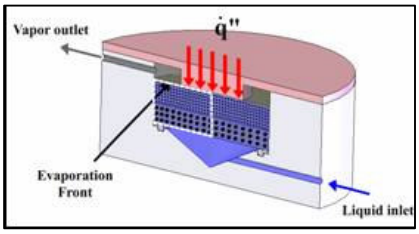

Figure 1a. Cut of the flat capillary evaporator with wick in the disk form with two different materials.

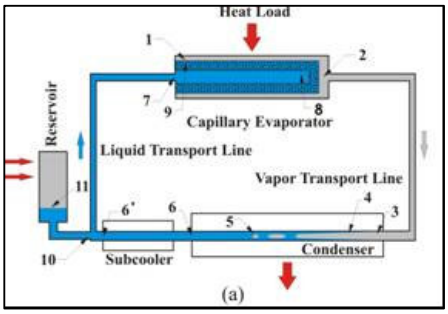

Figure 1b. Schematic diagram of a typical CPL.

The operation of the CPL shown in Fig. 1b can be described as follows. Heat is supplied to the evaporator so that the liquid saturating the surface pores of the wick evaporates, forming liquid-vapor curved interfaces. The curvature of these interfaces promotes the working fluid circulation by the action of capillary forces. The vapor, which has been generated into the evaporator, flows through the vapor line to the condenser, where heat is rejected to the atmosphere, causing the vapor to condense. Saturated liquid, before flowing back to the evaporator by pressure driven flow (essentially Poiseuille flow), is sub-cooled to prevent vapor bubbles of reaching the evaporator. The reservoir has the purpose of controlling the evaporation temperature of the system and to accumulate the liquid excess that is not being used in the loop. Detailed information on the operation, thermodynamic behavior, selection of working fluids and pressure losses of CPLs (Capillary Pumping Loop) and LHPs (Loop Heat Pipe) can be found in Santos and Bazzo (2007).

In this work, the wick is a flat circular disc and is assembled between the lines of liquid and vapor. The upper part of the wick is heated by an external heat flux. The evaporation process that takes place in the wick of the capillary evaporator depends on the applied thermal load on the system and occurs in three regimes: evaporation in microfilm, evaporation in the external surface of the wick and evaporation inside the wick. Here, the evaporation in the external surface is studied. This operation condition was verified experimentally by Li and Ochterbeck (1999), which mentioned also that seldom the evaporation occurs inside the wick. This hypothesis is assumed by Cao and Faghri (1994a), but it is not tested theoretically.

The calculation domain and the boundary conditions are represented schematically in Fig. 2. Due to the cylindrical symmetry of the evaporator, only the section represented by a dotted line in Fig. 1a is modeled.

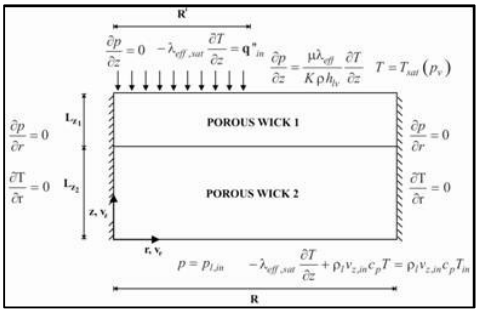

Figure 2. Schematic diagram of the calculation domain and the boundary conditions.

The model used here is an extension of Santos et. al. (2008), and a numerical solution for the regime of superficial evaporation front was obtained using the finite volume method. The equations of conservation of energy and of mass were cast in cylindrical coordinates. The following assumptions are made:

- the process is steady state;
- the porous layers forming the wick are isotropic and homogeneous;
- there is a negligible influence of gravity;

- there are no heat transfer by radiation nor energy generation (besides the phase change);
- the solid phase is inert and stationary;
- the fluid (liquid and its vapor) is incompressible;
- the thermophysical properties are constant;
- the solid phase is in local thermal equilibrium with the liquid phase;
- there are no chemical reactions.

The volume averaged equations for the conservation of mass of liquid, for incompressible fluid, in cylindrical coordinates is:

$$\frac{1}{r}\frac{\partial(r v_r)}{\partial r}+\frac{\partial v_z}{\partial z}=0 \tag{1}$$

where v_r and v_z are the r and z components of the velocity vector.

Here, the volume averaged notation (Kaviany, 1995) is omitted for simplicity. The formulation of the conservation of linear momentum equation depends on the presented flow velocity. It has been shown before (Demidov and Yatsenko, 1994; Cao and Faghri 1994a and Figus et. al., 1999) that the flow velocity in the application of interest here is small. From Santos et. al. (2008) it can be estimated that the pore Reynolds number ranges from $4.0\text{x}10^{-5}$ to $4.0\text{x}10^{-4}$. Therefore, macroscopic and microscopic (Forscheimer) inertia terms are negligible when compared to the microscopic viscous terms. Also, since boundary effects penetrate distances that are of the order of a few particle diameters, macroscopic (Brinkman) viscous term is also neglected. Finally, neglecting the influence of gravity, the r and z components of the equation for the conservation of linear momentum reduce to Darcy's Law, i.e.,

$$v_r=-\frac{K}{\mu}\frac{\partial p}{\partial r} \tag{2}$$

$$v_z=-\frac{K}{\mu}\frac{\partial p}{\partial z} \tag{3}$$

Substituting the conservation of momentum equation in the conservation of mass equation, we obtain,

$$\frac{1}{r}\frac{\partial}{\partial r}\left(r\frac{K}{\mu}\frac{\partial p}{\partial r}\right)+\frac{\partial}{\partial z}\left(\frac{K}{\mu}\frac{\partial p}{\partial z}\right)=0 \tag{4}$$

which reduces to a Laplace equation for the pressure when the properties are assumed constant.

The equation for the conservation of the thermal energy is also written neglecting the convective terms. Following Santos et. al. (2008), the characteristic Peclet number for the application of interest here is of the order of 10^{-2}. Then the equation for the conservation of thermal energy is written as,

$$\frac{1}{r}\frac{\partial}{\partial r}\left(r\lambda_{eff}\frac{\partial T}{\partial r}\right)+\frac{\partial}{\partial z}\left(\lambda_{eff}\frac{\partial T}{\partial z}\right)=0 \tag{5}$$

In the volume-averaged equation, and assuming local thermal equilibrium between the liquid and solid phases, λ_{eff} is the effective thermal conductivity of fully liquid saturated porous medium. For constant property, isotropic media, the conservation of thermal energy equation reduces to a Laplace equation for the temperature.

Following the system of coordinates (r,z) depicted in Fig. 2, the boundary conditions are as follows.

At the surface at r = 0, cylindrical symmetry requires that:

$$\frac{\partial p}{\partial r}=0 \quad and \quad \frac{\partial T}{\partial r}=0 \tag{6}$$

At the surface at r = R the boundary is assumed impermeable to liquid flow and adiabatic. Then,

$$\frac{\partial p}{\partial r}=0 \quad and \quad \frac{\partial T}{\partial r}=0 \tag{7}$$

At the inlet surface at z = 0, a prescribed pressure and a convective heat flux is assumed, i.e.,

$$p=p_{l,in} \quad and \quad -\lambda_{eff}\frac{\partial T}{\partial z}+\rho_l v_{z,in}c_p T=\rho_l v_{z,in}c_p T_{in} \tag{8}$$

This boundary condition reflects the continuity of the total normal component of the heat flux vector. Finally, at the outlet surface, two regions are observed. First, underneath the metallic fin ($z=L_z$ *and* $0\le r\le R'$),

$$\frac{\partial p}{\partial z}=0 \quad and \quad -\lambda_{eff}\frac{\partial T}{\partial z}=q''_{in} \tag{9}$$

Second, at the outlet surface, assuming that the pore size is not extremely small, i.e., this is not a hygroscopic porous medium, from Kelvin's Law, the surface temperature is approximately equal to the vapor saturation temperature in the bulk of the vapor channel. Also, the conduction heat transfer from the fin is responsible for the liquid evaporation. Therefore, we have,

$$\frac{\partial p}{\partial z} = \frac{\mu \lambda_{eff}}{K \rho h_{lv}} \frac{\partial T}{\partial z} \quad and \quad T = T_{sat}\left(p_v\right) \tag{10}$$

This set of boundary conditions close the formulation. The pressure difference $\left(p_v - p_{l,in}\right)$ corresponds to the total pressure loss of the CPL components. In all stable operation points, this pressure difference balances exactly the capillary pressure difference across the medium. The total heat transfer rate at the fin is responsible for the liquid evaporation at the outlet surface and part of it flows to the liquid channel. A total energy balance in the wick provides:

$q_{in,f} = q_{out,l} + q_{lv}$

where $q_{in,f}$ is the heat transfer rate at the fin surface,

$q_{in,f} = q"_{in,f}\, A_{in,f}$

The heat transfer rate to the liquid channel $q_{out,l}$ is given by,

$q_{out,l} = \int_0^R \left(-\lambda_{eff,sat} \frac{\partial T}{\partial z} \right) rdr$, at z = 0.

The heat transfer rate actually used for the liquid evaporation is,

$q_{lv} = \int_{R'}^R \left(-\lambda_{eff,sat} \frac{\partial T}{\partial z} \right) rdr$, at z = L_z.

Note that the total liquid mass flow rate is,

$$\dot{m}_{lv} = \int_{R'}^R \left(-\frac{K}{\mu} \frac{\partial p}{\partial z} \rho_l \right) rdr \text{ , at z = } L_z \text{, or, } \dot{m}_{lv} = \int_0^R \left(-\frac{K}{\mu} \frac{\partial p}{\partial z} \rho_l \right) rdr \text{ , at z = 0,} \tag{11}$$

The pumping capacity of a given porous wick is maximized when $q_{out,l}$ is minimized, i.e., when there is a smaller heat transfer loss to the liquid channel. Also, when $q_{out,l}$ is large, the liquid in the channel can reach the onset of nucleate boiling which is called a boiling limit for the CPL operation.

In the evaporation front (liquid-vapor interface), located in the external surface of the wick, the pressure difference between the phases liquid and vapor is the capillary pressure, which in its turn, can be expressed by the Young-Laplace's equation ($\Delta p_{cap} = p_v - p_l = \frac{2\sigma \cos\theta}{r}$). For an averaged radius of curvature *r* of the liquid-vapor interfaces, the capillary pressure becomes maximum when the contact angle between the liquid and the solid approaches zero, in other words, when the wettability of the working fluid is maximum. Since the objective of this paper is to explore the maximum pumping capacity, the contact angle is considered equal to zero. At the evaporation interface, the capillary pressure is defined by the liquid and vapor pressure. Then, the average radius of curvature of the liquid-vapor interface adjusts itself in order to balance this capillary pressure, as predicted by Young-Laplace's equation above. The minimum possible radius of curvature before drying of the pore is the characteristic radius of the pore. This radius depends on pore topology and is determined by the choice of material and manufacturing process, i.e., sintering, used to produce the porous wicks. The maximum capillary pressure that the wick can withstand is therefore,

$$\Delta p_{cap,max} = \frac{2\sigma}{r_p} \tag{12}$$

where r_p is the characteristic average pore radius of the pore structure. This characteristic average pore radius for the pore structure is related to the threshold for percolation of the non-wetting phase and is commonly identified, by Young-Laplace, to the wick bubbling pressure.

In the operation of a capillary evaporator, when the pressure losses of the system exceed the maximum capillary pressure, the system fails. Therefore, the capillary limit of a CPL reflects this maximum pumping capacity. Since the evaporation front is located in the external surface of the wick, the capillary pressure can be calculated by the difference between the saturation pressure of the vapor side and the pressure of liquid side.

3. NUMERICAL PROCEDURE

The conservation equations were solved numerically by the finite volume method (Maliska, 2004). The tri-diagonal matrix algorithm (TDMA) was employed to solve the discretized equations. The overall numerical algorithm is:

(1) First, an inlet velocity is estimated to solve the Laplace equation for the temperature. From the solution for T, the outlet velocity is calculated using the boundary condition of Eq. (10).

(2) Next, the pressure equation is solved using the outlet velocity calculated in (1). Then, the velocities are calculated and the values are compared to the ones obtained in step (1);

(3) Return to step (1) until the converged solution is obtained.

The grid independence has been studied, and it was found that a grid of (90x90) is sufficient to obtain independence. Convergence was examined by checking the overall mass and energy balances over the domain. The coupled equations are assumed to converge when overall energy and mass balances are satisfied within ± 1%.

4. RESULTS AND DISCUSSION

For the results presented here, water was used as a working fluid. A ceramic wick, primarily with one layer and next with two layers with different thermal properties was used as porous wick. The properties of the wick and the working fluid are presented in Tab. 1 and 2, respectively.

Table 1 Wick properties.

	ε	K (m^2)	$\lambda_{eff,1}$ (W/m-K)	$\lambda_{eff,2}$ (W/m-K)	r_p (μm)
Ceramic	0.50	$35x10^{-15}$	6.00	4.00	3.0

Table 2 Working fluid properties.

	σ (N/m)	h_{lv} (kJ/kg)	c_p (kJ/kg-K)	ρ (kg/m^3)	μ (kg/ms)
Water	0.07119	2382	4.18	995.6	0.0007977

Figure 3a presents the streamlines and isobaric lines (Pa) for the flow within the wick for an inlet heat flux of $4.0x10^4$ W/m^2, for water and a ceramic wick with $\lambda_{eff,1} = \lambda_{eff,2} = 4.0$ (W/m-K). This heat flux applied is representative of typical values in aeroespacial applications. The dimensions of the wick are: R = 15 mm, R' = 7.5 mm, $L_{z,1}$ = 4 mm, $L_{z,2}$ = 6 mm. The saturation temperature and the pressure at liquid inlet are T_{sat} = 40 °C and $P_{l,in}$ = 4246 Pa, respectively. The streamlines point upwards up to the middle of the structure, where they begin to change direction towards the outlet of the wick. Note that the liquid pressure is not uniform at the outlet surface, but becomes a consequence of the normal heat flux at this surface. There is a strong curvature of the streamlines at the end of the fin (at $r = R'$). Figure 3b presents the inlet and outlet normal velocities. Note the high velocity of the vapor flow at the end of the fin.

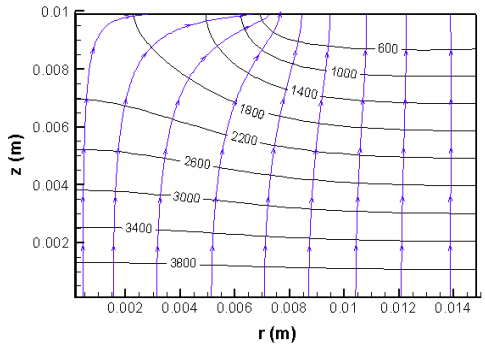

Figure 3a Streamlines and isobaric lines (Pa) in the wick for a heat flux of $4.0x10^4$ W/m^2.

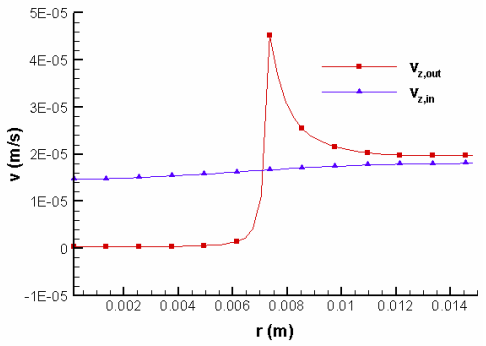

Figure 3b Inlet and outlet normal velocities for a heat flux of $4.0x10^4$ W/m^2.

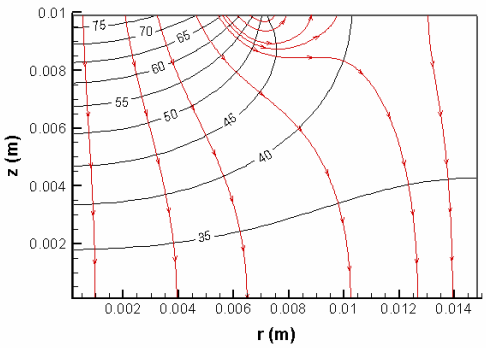

Figure 4a Isothermal lines (°C) and heat streamlines for a heat flux of $4.0x10^4$ W/m^2.

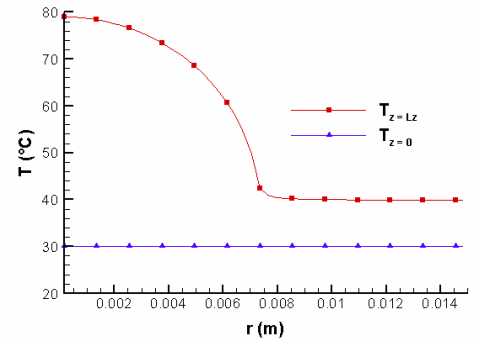

Figure 4b Temperature profiles at the inlet and outlet for a heat flux of $4.0x10^4$ W/m^2.

Figure 4a presents the isothermal and heat flux lines for an inlet heat flux of 4.0×10^4 W/m^2. Note that part of the heat flows to the outlet and the other part flows right to the feeding liquid channel. Figure 4b presents the temperature distribution at outlet and inlet for the same inlet heat flux used for the Fig. 4a. The inlet temperature appears to be a straight line, but it is not. Further on, there will be a graphic depicting this variation.

4.1 Effect of the magnitude of the external heat transfer rate in the mass flow rate

It is expected that an increase in the heat flux at the fin causes an increase in the mass flow rate. Figs. (5a), (5b) and (5c) present the isothermal and heat flux lines for three increasing heat fluxes. Figure 5a presents the results for an inlet heat flux of 2.0×10^4 W/m^2. The fin ends at r = 7.5 mm. Note that surface evaporation occurs only in the first few millimeters of the outlet surface. Very close to the end of the fin. The heat flux lines turn around and heat flows right to the liquid channel. As the heat flux is increased (Figs. 5b and 5c) an increased amount of heat flows to the outlet surface, causing the liquid evaporation.

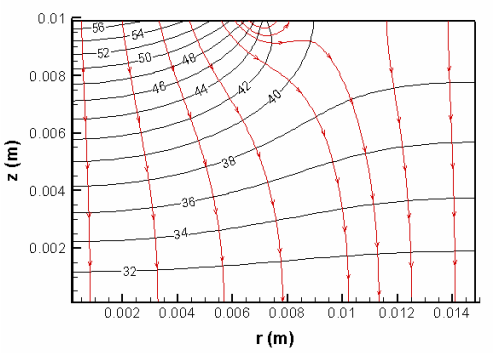

Figure 5a Isothermal (°C) and heat flux lines for an inlet heat flux of 2.0×10^4 W/m^2.

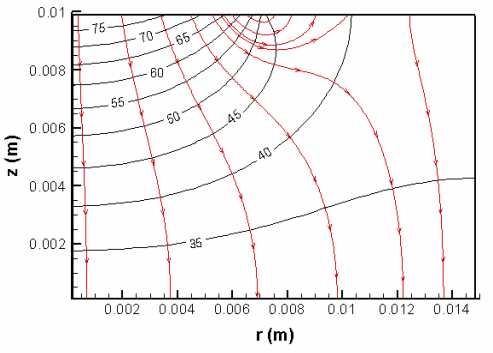

Figure 5b Isothermal (°C) and heat flux lines for an inlet heat flux of 4.2×10^4 W/m^2.

This is also evidenced in Fig. 6 that presents the normal liquid velocity at the outlet surface. The area underneath the curve shown is proportional to the mass flow rate. Since the normal velocity at region underneath the fin is zero, Fig. 6 depicts only the vapor outlet surface ($z = L_z$ *and* $R' \le r \le R$).

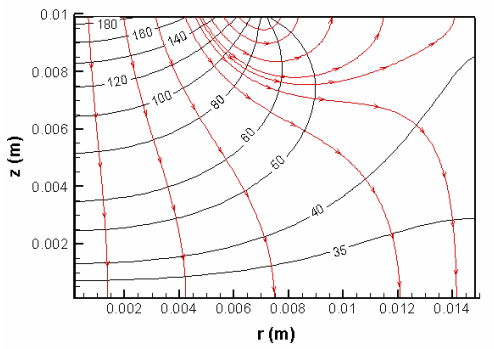

Figure 5c Isothermal (°C) and heat flux lines for an inlet heat flux of 1.4×10^5 W/m^2.

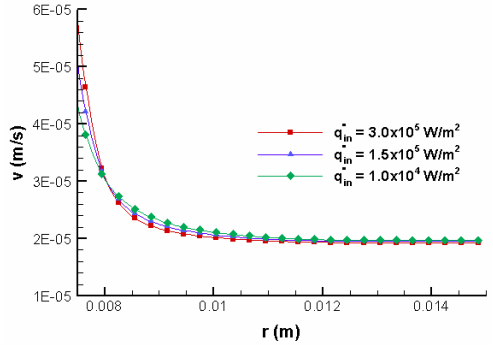

Figure 6 Normal liquid velocity at the outlet surface as a function of inlet heat flux.

4.2 Analysis of the onset of drying

The heat transfer rate imposed in the fin is transferred to the outlet surface, causing evaporation and also to the inlet surface resulting in heating of the liquid channel. Both theses heat transfer paths have their characteristic thermal resistances (two dimensional). As a result of theses thermal resistances, the fin surface reaches a temperature which can be reasonably large in certain conditions. For instance in Fig. 5c, we observe that for an inlet heat flux of 1.4×10^5 W/m^2 the fin surface reaches temperatures above 180 °C which are about 140 °C above the fluid saturation temperature (for infinite radius of curvature). Then, a question remains whether the fluid would remain liquid or evaporate under this temperature. This can be tested by observing the capillary pressure at the top surface of the wick and comparing it to the maximum capillary pressure that the wick can sustain.

Figure 7 presents the capillary pressure at the top surface as a function of properties for two heat fluxes and four characteristic average radius (from 3×10^{-6} m to 15×10^{-6} m). All properties were kept constant and correspond to the average pore radius of 3×10^{-6} m. The horizontal lines represent the maximum capillary pressure for each characteristic

pore size. We note that for the inlet heat flux of $2.0x10^4$ W/m^2 all medium would remain saturated by liquid except those with the larger porous of $10x10^{-6}$ m and $15x10^{-6}$ m. For these two sizes, the local capillary pressure exceeds the maximum allowed capillary pressure and, therefore, the region underneath the fin would dryout and the evaporation front would seek a new equilibrium position within the wick. This condition in which the front is embedded within the wick has been analyzed by Cao and Faghri (1994a), Demidov and Yatsenko (1994), Figus et al. (1999) and Kaya and Goldak (2006).

For higher heat flux, all media with pore sizes above $3x10^{-6}$ m would suffer dry out underneath the fin. Therefore, there is a relation between the pore size (and all medium properties) and the heat flux at the onset of drying. Note that this drying underneath the fin may not cause the failure by the capillary limit, since there may be a stable condition for operation with the embedded evaporation front. This, however, is not analyzed here.

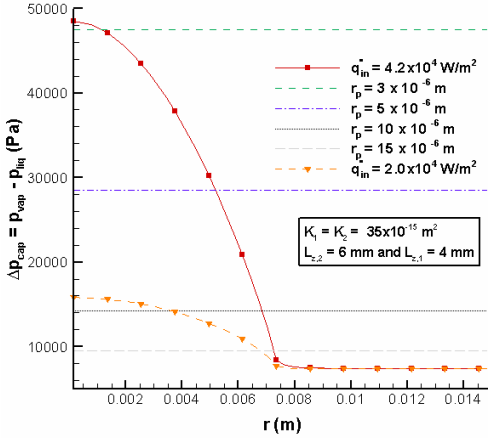

Figure 7 Capillary pressure profiles at z = L_z for different averaged radius of curvature and inlet heat fluxes.

4.3 Analysis of a bi-layered structure on inlet temperature and onset of drying

Here, the analysis of the porous wick with two layers is presented. It is expected that this kind of porous structure improves the capillary pumping capacity, avoiding reaching the capillary limit. It is also expected that the heat transfer to the feeding liquid channel is decreased. For the bi-layered porous wick, porous wick 1 and 2 have lengths of $L_{z,1}$ = $4x10^{-3}$ m and $L_{z,2}$ = $6x10^{-3}$ m, respectively. The porous wick 2 has the effective thermal conductivity constant ($\lambda_{eff,2}$ = 4.0 W/m-K). The effective thermal conductivity of the porous wick 1 was varied in order to evaluate its effect on the onset of drying and inlet temperature.

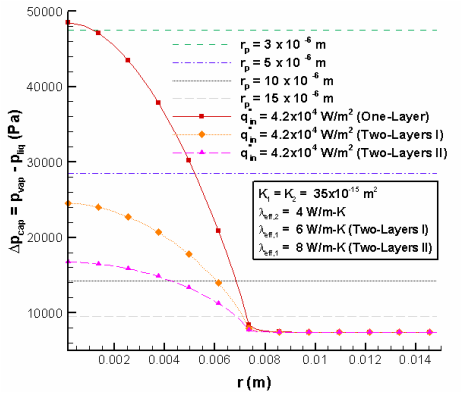

Figure 8 Capillary pressure profiles at z = L_z in the bi-layered wick for different averaged radius of curvature and inlet heat fluxes.

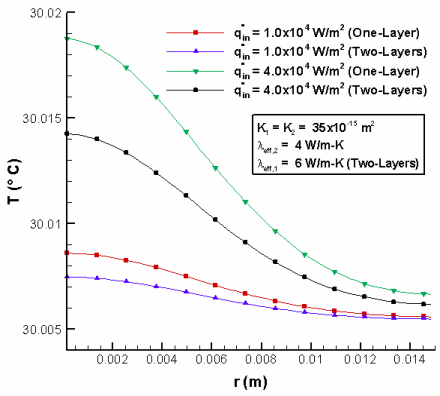

Figure 9 Inlet heat flux of the wick for different thermal conductivities for a fin radius.

Figure 8 presents the capillary pressure at the top surface as a function of properties of the wicks with one and two layers for an inlet heat flux of $4.2x10^4$ and four characteristic average radius (from $3x10^{-6}$ m to $15x10^{-6}$ m). All properties were also kept constant and correspond to the average porous radius of $3x10^{-6}$ m. We note that for the inlet heat flux of $4.2x10^4$ W/m^2 in the wick with two layers, as the thermal conductivity increase the local capillary pressure decreases and may not exceed the maximum allowed capillary pressure. Therefore, we should manufacture porous wicks with these characteristics in order to avoid the drying of the region underneath the fin. Figure 9 presents the variation of the inlet temperature as a function of the inlet heat flux for porous wicks with one and two layers. As expected, we observe that the temperature distribution at inlet of the wick with one layer is higher than the temperature

distribution of the wick with two layers. Nevertheless, the differences between the temperature distributions are small. Therefore, the onset of nucleate boiling which is called a boiling limit for the CPL operation either does not occurs for both porous wicks.

5. CONCLUSION

The numerical resolution of the model was able to simulate the heat and mass transfer within a wick with one and two layers with different thermophysical properties. This model improved the boundary condition in the vapor outlet, which the velocity is not uniform as it was assumed by Santos et. al. (2008). The results show that the velocity at outlet is high close to the fin and its value decreases from the region close to the fin to the region distant. The analysis of the wick with one and two layers showed that the wick with two layers is better than with one layer, regarding the onset of drying underneath the fin. Further conclusions are: i) The capillary limit, or onset drying, has a relation between the pore size (and all medium properties) and the heat flux. If this limit is reached, the evaporation front enters into the wick. ii) The larger the thermal conductivity of the porous wick 1 (underneath the fin), the smaller is the heat transfer to the feeding channel, causing a smaller increase of the inlet temperature. But the increase of the inlet temperature was small under the conditions here. The increase of the thermal conductivity of the porous wick 1 causes the increase of the capillary limit, avoiding the onset dry of the region underneath the fin. The increase of the thermal conductivity also decreases the mass flow rate, causing the decrease of the pressure losses through the porous wick. iii) Finally, the dimensions of the bi-layered wick ($R = 15$ mm, $R' = 7.5$ mm, $L_{z,1} = 4$ mm, $L_{z,2} = 6$ mm) and its thermophysical properties can be used for a design of a capillary evaporator.

Therefore, according to theses results presented here, we can conclude that the model allowed to verify whether the evaporation front is actually located at the upper surface of the wick or it is embedded into the wick. That is, this model ensures that for a maximum inlet heat flux, the evaporation front is located at the upper surface of the wick. However, even if the evaporation front is embedded into the wick, this may not cause the failure of the capillary evaporator by the capillary limit, because there may be stable conditions for operation with the embedded evaporation front.

6. ACKNOWLEDGEMENTS

The authors thank the National Council for Scientific and Technological Development (CNPq), a foundation linked to the Ministry of Science and Technology (MCT) to support Brazilian research.

7. REFERENCES

Cao, Y. and Faghri, A., 1994 (a), “Conjugate analysis of a flat-plate type evaporator for capillary pumped loops with three-dimensional vapor flow in the groove”, Int. J. Heat Mass Transfer, vol 37, issue 3, pp 401-409.

Cao, Y. and Faghri, A., 1994 (b), “Analytical Solution of Flow and Heat Transfer in a Porous Structure with Partial Heating and Evaporation on the Upper Surface”, Int. J. Heat Mass Transfer, vol 37, issue 10, pp 1525 - 1533.

Demidov, A. S. and Yatsenko, E. S., 1994, “Investigation of Heat and Mass Transfer in the Evaporation Zone of a Heat Pipe Operating by the ‘Inverted Meniscus’ Principle”, Int. J. Heat and Mass Transfer, vol 37, issue 14, pp 2155-2163.

Figus, C., Bray, Y. Le, Bories, S. and Prat, M., 1999 “Heat and Mass Transfer with phase change in a porous structure partially heated: Continuum Model and Pore Network Simulation”, Int. J. of Heat and Mass Transfer, vol 42, pp 2557 – 2569.

Kaya, T. and Goldak, J., 2006, “Numerical analysis of heat and mass transfer in the capillary structure of a loop heat pipe”, Int. J. Heat Mass Transfer, vol 49, pp 3211-3220.

Kaviany, M., 1995 “Principles of Heat Transfer in Porous Media”, 2nd edition, Springer-Verlag New York, Inc.

Li, T. and Ochterbeck, J. M., 1999, “Effect of Wick Thermal Conductivity on Startup of a Capillary Pumped Loop Evaporator”, AIAA paper Nº 993446.

Maliska, C. R., 2004, “Transferência de Calor e Mecânica dos Fluidos Computacional”, 2 ed. Rio de Janeiro: Livros Técnicos e Científicos Editora.

Santos, P. H. D. and Bazzo, E., 2007, “Thermohydraulic Analysis of Two-Phase Capillary Pumping Systems for Industrial Design and Space Applications”, Proccedings of the 19th International Congress of Mechanical Engineering (COBEM), Brasília, Brasil.

Santos, P. H. D., Bazzo, E. and Oliveira, A. A. M., 2008, “Solução Analítica para os Campos de Temperatura e de Velocidade na Estrutura Porosa de um Evaporador Capilar”, Proccedings of the 5th National Congress of Mechanical Engineering (CONEM), Bahia, Brasil.

8. RESPONSIBILITY NOTICE

The author(s) is (are) the only responsible for the printed material included in this paper.